

Bimorph electrothermal micro-gripper with large deformation, precise and rapid response, and low operating voltage

Cite as: Appl. Phys. Lett. 121, 023502 (2022); <https://doi.org/10.1063/5.0100920>

Submitted: 27 May 2022 • Accepted: 24 June 2022 • Published Online: 11 July 2022

 Xusheng Hui, Jianjun Luo, Xinliang Wang, et al.



View Online



Export Citation



CrossMark

 QBLOX



1 qubit

Shorten Setup Time

Auto-Calibration

More Qubits

Fully-integrated

Quantum Control Stacks

Ultrastable DC to 18.5 GHz

Synchronized <<1 ns

Ultralow noise



100s qubits

[visit our website >](#)

Bimorph electrothermal micro-gripper with large deformation, precise and rapid response, and low operating voltage

Cite as: Appl. Phys. Lett. **121**, 023502 (2022); doi: [10.1063/5.0100920](https://doi.org/10.1063/5.0100920)

Submitted: 27 May 2022 · Accepted: 24 June 2022 ·

Published Online: 11 July 2022



View Online



Export Citation



CrossMark

Xusheng Hui,¹ Jianjun Luo,^{1,a)} Xinliang Wang,¹ Rong Wang,¹ and Hao Sun^{2,a)}

AFFILIATIONS

¹School of Aeronautics, Northwestern Polytechnical University, Xi'an, Shaanxi 710072, China

²School of Mechanical Engineering, Tsinghua University, Beijing 100084, China

^{a)}Authors to whom correspondence should be addressed: jjluo@nwpu.edu.cn and haos@mail.tsinghua.edu.cn

ABSTRACT

Micro-grippers are highly desired in engineering, robotics, and biomedicine. However, on the basis of satisfying the requirements of miniaturization, precise manipulation, and low power consumption, the existing micro-grippers are difficult to achieve rapid response simultaneously. In this paper, we present a bimorph electrothermal micro-gripper that composed of several metal ultrathin films with high surface-to-volume ratios, allowing rapid heating and cooling processes. Patterns of these films are exquisitely designed so that the micro-gripper naturally forms an embedded circuit to optimize the current distribution. The micro-gripper can be precisely actuated under voltages below 2 V, while dramatically responding to pulse voltages up to 100 Hz. By interacting with a silica particle 96 times heavier than its weight, potential applications of the micro-gripper in robotics, organic tissue engineering, and interventional surgery can be shown. The advantage to be compatible with other semiconductor components ensures that the functions of the micro-gripper can be further expanded.

Published under an exclusive license by AIP Publishing. <https://doi.org/10.1063/5.0100920>

Micromanipulation is attracting considerable critical attention in engineering, robotics, and biomedicine. Although many hard grippers with rigid joints have been developed to manipulate objects precisely and effectively,^{1–3} soft grippers using pneumatic,^{4,5} hydraulic,^{6–8} and electrical actuation⁹ are still highly desired to provide protective interaction with soft and fragile objects with various shapes. With the rapid development of MEMS, miniaturization of the sensors and actuators including micro-grippers has made great progress.¹⁰ Smart film micro-grippers capable of responding to electricity,¹¹ light,¹² temperature,^{13,14} air pressure,¹⁵ and pH of resolution¹⁶ have shown great advantages in miniaturization because of their compatibility with the MEMS technique. This characteristic guarantees their broad applications in biomedicine, such as organic tissue isolation,^{17,18} cell screening and manipulation,^{19–21} drug delivery,^{16,22} and interventional medical surgery.^{23,24} Polymer hydrogel is currently the most commonly used smart material for micro-grippers due to its superior biocompatibility and programmability.^{25,26} However, hydrogel-based micro-grippers are highly dependent on an aqueous environment for actuation and always face the problems of low stiffness and slow response.¹⁹ Much of the current research on micro-grippers pays particular attention to their large strain, precision, and miniaturization, while ignoring the importance of response speed. For biomedical

applications, the ability of fast response is essential when it comes to providing a high shear rate needed to reduce blood viscosity for thrombus removal.²⁷ Smart micro-actuators responding to electrical signal show great advantages in terms of response speed compared with other external stimuli.^{28–30} Micro-grippers based on dielectric elastomer can respond at a high speed but require operating voltages up to thousands of volts.³¹ Electromagnetic micro-grippers also face the problems of high structural complexity and high operating voltages, which are not conducive to miniaturization and biomedical applications.³² Although piezoelectric micro-grippers have significant advantages in fast response, the displacement caused by deformation is extremely small and the driving voltage is high.³³ Therefore, it still remains a grand challenge to achieve a micro-gripper that takes miniaturization, large deformation, low operating voltage (low-power), and precise and rapid response into consideration simultaneously.^{34–36}

In this paper, we proposed a bimorph electrothermal micro-gripper, which can be electrically actuated to produce a precise and rapid response with large deformation under low excitation voltage. First, the design scheme and the actuation mechanism of the micro-gripper were introduced. Then, the fabrication processes of the micro-gripper through MEMS technique were sequentially described.

Following this, several experiments were carried out to investigate the performance of the micro-gripper under electrical actuation. Finally, a demonstration experiment of the micro-gripper interacting with a target particle was performed to prove its basic operability and controllability.

As shown in Fig. 1(a), the micro-gripper is composed of a main body, two electrode pads, and two linkage beams for mechanical and electrical connections. The main body of the micro-gripper is made of two metal/alloy layers: the aluminum film (thickness: 400 nm) and the nitinol film (thickness: 500 nm). The main advantages of this metal couple are (1) that large difference in coefficients of thermal expansions (CTEs) contributes to the large deformation of the micro-gripper, (2) that the low electrical resistivity of aluminum facilitates the formation of embedded circuits and optimization of current paths, (3) that good oxidation resistance of the nickel base alloys and the dense oxide film on the aluminum protects the micro-gripper from damage during the etching process, and (4) that these two materials have good biocompatibility. Sharing the aluminum film with the main body through linkage beams, the electrode pads are made of additional

gold films to prevent oxidation. The major concern of this planar design scheme is that it allows us to adopt the MEMS technique for manufacturing, which brings us numerous benefits, such as miniaturization, parallel manufacturing, and compatibility with other semiconductor components. After the deposition of these films, bimorph micro-laminates are obtained and the temperature difference leads to the bending deformation of each blade due to the mismatch of the CTEs of different materials [Fig. 1(c)]. We use R , the distance between the axis of the micro-gripper and the end of the blade in Figs. 1(c) and 1(d) as the index to measure the deformation of the micro-gripper in the following passage, which can be expressed as follows:

$$R = R_0 + \rho \sin \frac{L}{\rho}, \quad (1)$$

where R_0 is the distance from the central axis of the micro-gripper to the root of the blade, ρ is the radius of curvature of the blade after deformation, and L is the length of the blade [Fig. 1(d)]. According to Timoshenko,³⁷ the radius of the curvature of a bimorph to the uniform heating can be expressed as

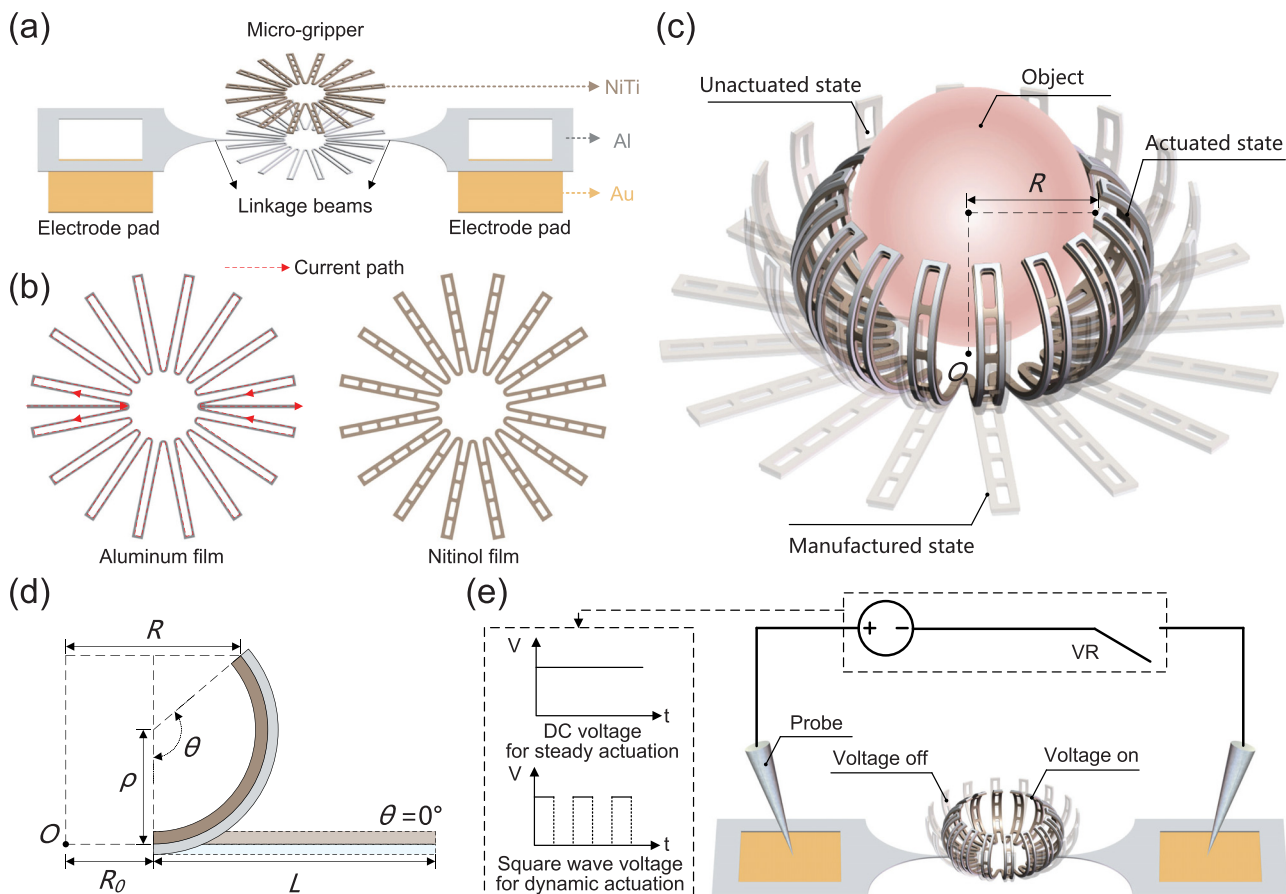


FIG. 1. (a) Explosion view of the micro-gripper which composed of three layers of gold, aluminum, and nitinol ultrathin films. (b) Design profiles of the aluminum and nitinol films. The red dashed arrow indicates the current path in the aluminum film. (c) Schematic of the micro-gripper at the planar state after released, unactuated pre-deformed state after heat treatment, and the actuated state with an object inside. (d) Definition of the bending deformation of the micro-gripper illustrated in the cross section view of one blade. (e) Schematic of the electrical actuation system of the micro-gripper.

$$\rho = \frac{h \left[3(1+m)^2 + (1+m) \left(m^2 + \frac{1}{mn} \right) \right]}{6(1+m)^2(\alpha_2 - \alpha_1)\Delta T}, \quad (2)$$

where $m = t_1/t_2$ is the ratio of the thicknesses of these two films, $h = t_1 + t_2$ is the total thickness of the films, $n = E_1/E_2$ is the ratio of Young's modulus of the two materials, α_1 and α_2 are the coefficients of the thermal expansion of the two materials, and ΔT is the temperature difference. Subscripts 1 and 2 represent the nitinol and the aluminum film, respectively.

The micro-gripper is connected to a DC power through the contact between the probes and the electrode pads for simple and stable electrical connection in the current experimental stage. After applying electrical power, the structural temperature of the micro-gripper will increase due to the Joule heat, which leads to the bending of the blades [Fig. 1(e)]. After applying electrical power, the structural temperature of the micro-gripper will increase due to the Joule heat, which lead to the bending of the blades. Therefore, under the excitation of DC driving voltages and square-wave pulse voltages, the micro-gripper can extend and shrink steadily and repeatedly [Fig. 1(e)]. The square-wave pulse voltages are obtained by the rectification of the DC voltages using a voltage relay (VR) [Fig. 1(e)]. A star-like pattern is designed for the aluminum film to form an embedded series-parallel circuit and the same pattern is designed for the nitinol film with additional reinforcing ribs to enhance the mechanical strength of the micro-gripper and to improve the synchronization of all parts of the micro-gripper during the etching process [Fig. 1(b)]. Because the resistivity of aluminum ($2.7 \times 10^{-4} \Omega/\text{m}$) is much less than that of Nitinol ($8.2 \times 10^{-3} \Omega/\text{m}$), the aluminum film layer can distribute most of the

current. The embedded circuit in the aluminum film guarantees that the current flows through the end of micro-gripper, avoiding localized overheating in the center area [Figs. 1(b) and 3(b)]. Benefit from this optimization of the current path and the high surface-to-volume ratio of the ultrathin films, the micro-gripper is expected to perform fast heating and cooling response under low voltages.

To fabricate the designed micro-gripper, a series of MEMS manufacturing processes, such as the electron beam (E-beam) evaporation process, the inductively coupled plasma chemical vapor deposition (ICPCVD) process, the photoresist liftoff process, and the isotropic dry etching process, were involved. Starting with a 4-in. p-type silicon wafer, the photoresist (AZ5214) was spin-coated and exposed to UV light [Fig. 2(a-i)]. After development, the removal parts of the photoresist formed the expected patterns with an accuracy of 500 nm. A 100 nm gold film was then deposited on the surface of the wafer by the E-beam evaporation [Fig. 2(a-ii)]. After soaking in an organic solution (N-methylpyrrolidone, NMP) at 85°C for 2 h, the rest photoresist with gold deposited on its surface was lifted off, leaving a patterned gold film on the wafer surface [Fig. 2(a-iii)]. Similar processes were repeated to sequentially deposit patterned aluminum, nitinol, and SiO₂ films, except for the deposition method of the SiO₂ film was ICPCVD [Figs. 2(a-iv)–2(a-ix)]. High-precision pattern transformation for multilayer films could be achieved thanks to the perfect directivity of the E-beam deposition and the low temperature process of ICPCVD. The obtained SiO₂ film only worked as an etching mask that covered most of the wafer surface, leaving several exposed areas around the micro-gripper to improve the etching efficiency [Figs. 2(a-ix) and 2(b)]. After the isotropic dry etching process using XeF₂, the deformation part of the micro-gripper was safely released

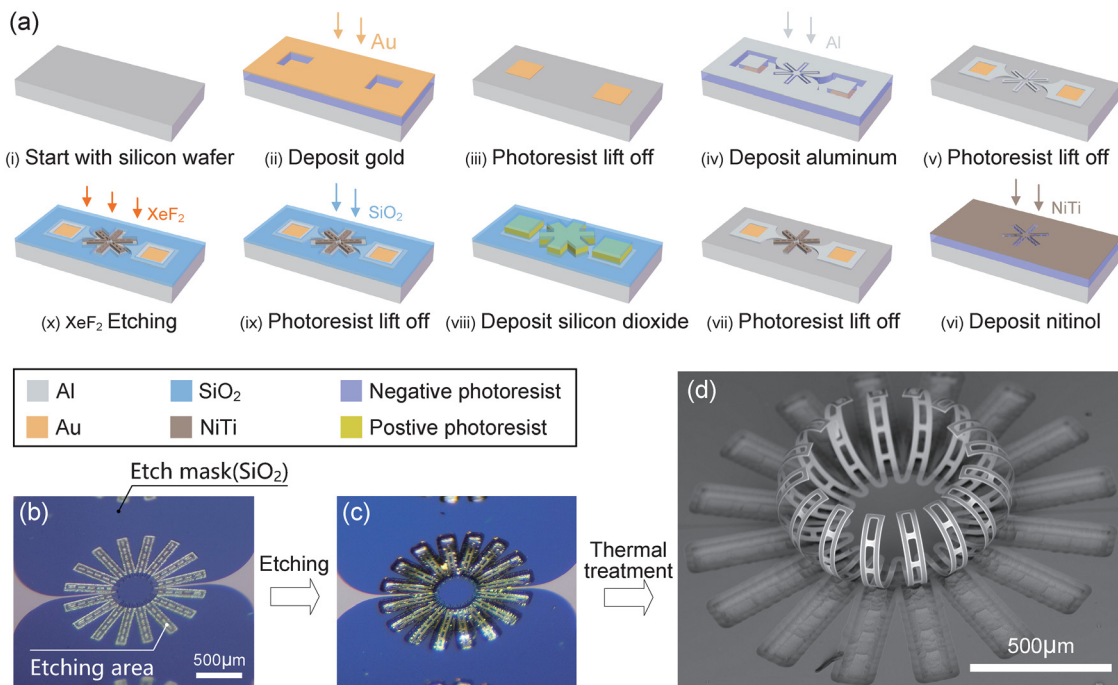


FIG. 2. (a) Fabrication process flow of the micro-gripper based on the MEMS technique. Microscope photographs of the micro-gripper (b) at the planar state before etching and (c) at the reversely bending state after etching. (d) A scanning electron microscopy (SEM) photograph of the micro-gripper at the pre-deformed state after heat treatment.

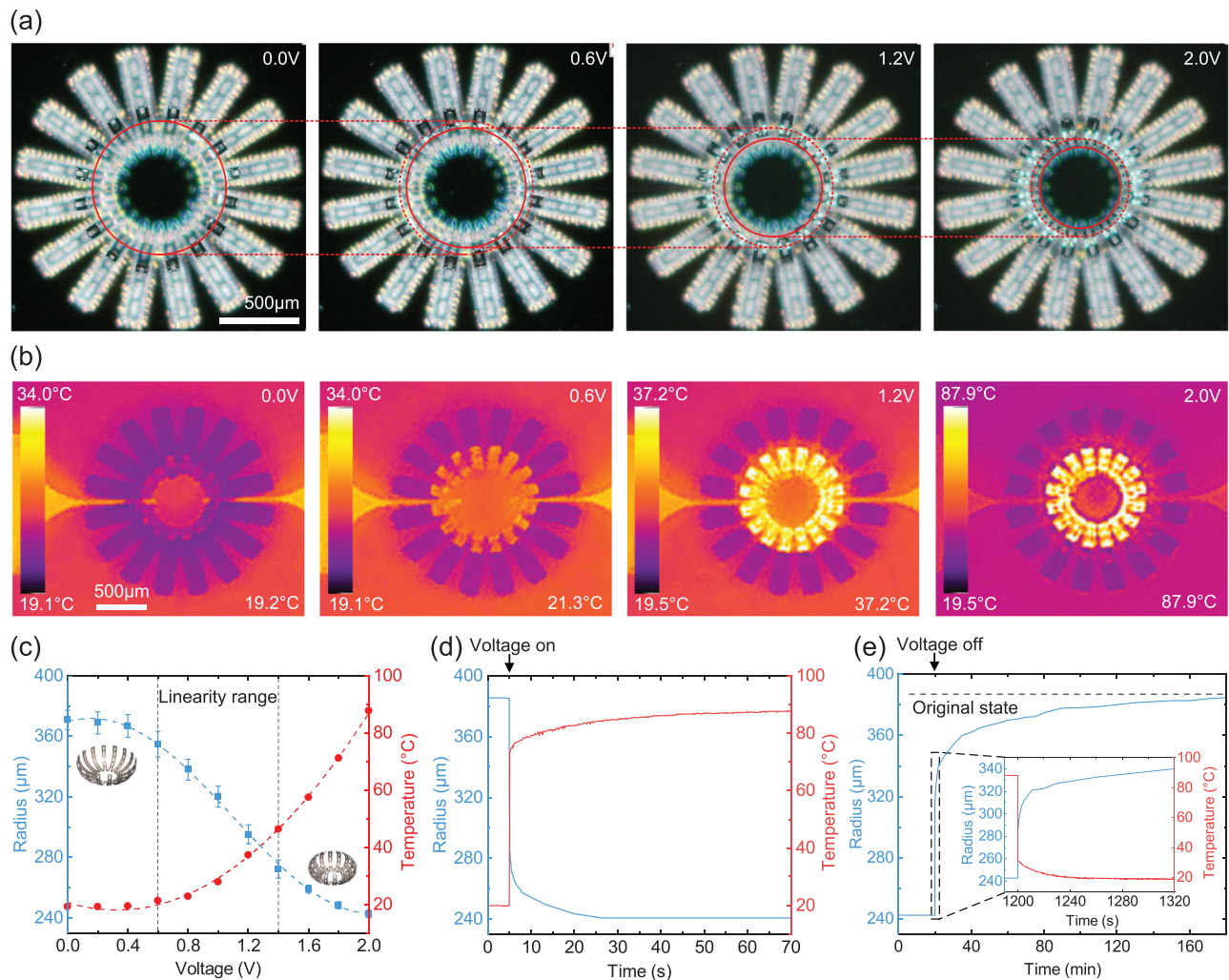


FIG. 3. (a) The steady-state response of the micro-gripper under DC voltages. The red solid circles represent its opening profile under the current voltage, and the red dashed circles indicate its opening profile under the former voltage. (b) IR camera images of the micro-gripper viewed from the top under DC voltages. (c) Radius–temperature–voltage graph of the micro-gripper. (d) Variation of the radius and the temperature of the micro-gripper after a voltage of 2 V was applied. (e) Variation of the radius and the temperature of the micro-gripper after the power was cut off. The internal illustration captured the variation within the first 60 s after the power was cut off.

from the wafer, avoiding the damage to the structure by liquid surface tension compared with the wet etching technique [Fig. 2(c)]. In addition to their large difference in coefficients of thermal expansion, the reason why we choose aluminum and nitinol is their strong oxidation resistance, which prevent the micro-gripper from being damaged during the etching process. In order to eliminate the residual stress generated during the deposition process, micro-grippers were then heat treated in a furnace filled with argon at 200 °C for 1 h. After that, the reverse bending trend was corrected and the micro-gripper was pre-shaped to shorten the driving distance during the subsequent electrical actuation experiments [Fig. 2(d)].

After manufacturing, we investigated the response of the micro-gripper under DC and square-wave voltages to evaluate its mechanical and thermodynamic behaviors. The investigation was performed through the system shown in Fig. 1(e). As the most important index

for measuring the deformation, the radius of the micro-gripper was photographed and measured through a microscope from the top view. Figure 3(a) shows a series of microscope images of the micro-gripper taken under DC voltages from 0 to 2 V in which a significant shrink could be observed. During this test, the radius of the micro-gripper decreased from 385.4 to 240.6 μm (i.e., a 37.6% contraction) and the maximum current was only 38.16 mA (i.e., 76.32 mW). The miniaturized ultrathin metal film contributes to the low driving voltage due to its sensitivity to electric heating. Lower driving voltage means lower requirements on the actuation system when it comes to wireless energy supply, as well as safer working conditions when it comes to biomedical applications in the future work. As shown in Fig. 3(b), the temperature distribution of the micro-gripper was quite uniform after a voltage was applied, confirming the effectiveness of the embedded circuit design method for the optimization of the current path.

As shown in Fig. 3(c), there was a significant trigonometric correlation between the radius and the voltage applied. What stands out in the figure is this specific range between 0.5 and 1.5 V where the radius decreased linearly with the increase in voltage, guaranteeing the application prospect of the micro-gripper in the high precision micromanipulation. Outside the linearity region, there are two nonlinear regions in which the radius of the micro-gripper was insensitive to the changes in the actuation voltages. This is because the central angles of the micro-gripper were around 90° and 270°, respectively, and the projection of the bending deformation on the radius plane was rather small. In these nonlinear regions, the micro-gripper has better anti-interference ability and robustness for the manipulation and transfer of the target in the post-grasping process. It can also be seen from Fig. 3(c) that the maximum temperature of the micro-gripper could be maintained below 37.4 °C under the excitation of the DC voltage below 1.2 V, which was close to human body temperature and harmless to the living organism. This result proves the feasibility of the micro-gripper in biomedical applications.

Rapid response of the micro-gripper is also important for biomedical applications, such as providing a high shear rate needed to reduce the blood viscosity for the thrombus removal.²⁷ For most thermal actuators, the slow heating and cooling processes greatly limit their response speed and practical applications. In this paper, the designed embedded circuit in the micro-gripper effectively optimized the current path to the end of the blades, avoiding localized overheating in the center area [Fig. 3(b)]. After a voltage of 2 V was applied, the temperature of the micro-gripper rose 50 °C in 0.1 s and reached steady state after 60 s. The radius of the micro-gripper decreased at the same rate as the temperature rose [Fig. 3(d)].

In fact, many thermal actuators do increase their structural complexity and weight in exchange of a slight improvement in cooling speed, such as active heat dissipation and cooling media.³⁸ In this paper, air convention was the only way for heat dissipation and no active method was involved. Under this condition, the heat dissipation power Q of the micro-gripper can be expressed as

$$Q = hA(T - T_{env}), \quad (3)$$

where h is the heat transfer coefficient ($\text{W}/\text{m}^2 \text{ K}$), A is the heat transfer area, T and T_{env} are temperatures of the micro-gripper and the environment, respectively. From Eq. (2), we can see that the larger the surface, the faster the heat dissipation. The thicknesses of the films obtained by E-beam were about several hundred nanometers. Therefore, the micro-gripper should have a pretty high surface-to-volume ratio and a fast theoretical cooling rate. As shown in Fig. 3(d), after the micro-gripper reached steady state at an applied voltage of 2 V, the power was cut off and the temperature dropped dramatically from 87.9 to 28 °C within 0.1 s, indicating a rapid cooling rate. However, the recovery of the radius of the micro-gripper lagged significantly behind the temperature drop. It only recovered 37% of the deformation within 0.1 s and 50% of the deformation within 6.5 s compared to the initial state [Fig. 3(d)]. The main reason for this phenomenon is probably the anelasticity caused by the time-varying elastic modulus of the materials, which will be further explored and improved in the future work.

Although it took considerable time for the micro-gripper to fully recover to its initial state, we do not necessarily need the

whole driving distance when it comes to high speed applications, such as hemodilution. According to Ranucci, the time-to-gel point (TGP) and maximum clot viscosity (MCV) of the blood during the coagulation process, which are important parameters associated with the occurrence of thromboembolic events, can be significantly affected by shear rates. A higher shear rate up to 80 s^{-1} will lead to lower TGP and MCV,²⁷ which should be an effective way for safer thrombus removal.

Therefore, dynamic performances of the micro-gripper were then fully investigated. Under the excitation of square-wave pulse voltages, the micro-gripper extended and shrank repeatedly. As shown in Fig. 4(a), considerable deformation of the micro-gripper could be observed at the pulse frequency of 10 Hz. In contrast to this, vibration with slight amplitude was hardly detected when the pulse frequency reached 100 Hz, indicating a strong relationship between the deformation ability of the micro-gripper and the frequency of the driving voltage [Fig. 4(b)]. In order to assess the detail dynamic characteristics of the micro-gripper, the responses at frequencies from 1 to 100 Hz were investigated. Figure 4(c) presents the scatter diagram of the relationship between the extreme value of the radius and the frequencies of driving voltages. The minimum and maximum radii represent the ultimate shrink ability and the extendable ability of the micro-gripper after one cycle of heat dissipation, respectively. It is obvious that the minimum radius decreased as the frequency increased during the repetitive oscillation process because of the shorter heating periods. For the maximum radius, it decreased with the increase in the frequency below 20 Hz, mainly because of the shorter cooling time to recover. Yet with the increase in the frequency over 20 Hz, the maximum radius increased because of the relatively high starting point for rebound due to the insufficient contraction in the heating period. The overall level of the maximum and the minimum radii decreased as the voltage amplitude increased, and the higher the voltage amplitude, the more drastic the change in the radius with changing frequency. Areas between the maximum and the minimum radii in Fig. 4(c) are the radius differences of the micro-gripper, which represents the driving distance. Radius differences gradually decreased and approached 0 as the frequency increased [Fig. 4(d)]. However, we noticed an unanticipated result that the radius differences of the micro-gripper under the voltage of 1.5 V were even higher than that at 2.0 V, which is evidence to prove that the driving distance is a compromise result between the shrinkage and extend capabilities. These experimental results confirmed that the micro-gripper was capable of performing multiple tasks. For micromanipulation tasks, such as tissue isolation and cell screening, DC voltages or pulse voltages with low frequencies enable the micro-gripper to take full advantages of its large deformation and precise response. For microfluidic control tasks, such as reducing the TGP and MCV of the blood, rapid response with considerable driving distance of the micro-gripper is highly desired.

To further validate the proposed micro-gripper from practical perspective, we experimentally demonstrated its ability to hold and lift certain spherical particles. As shown in Fig. 5, the target object (SiO_2 , ϕ 500 μm) was placed in the center of the micro-gripper. Under different levels of applied voltages, the micro-gripper was able to hold and control this target object 96 times heavier (0.157 mg) than its own weight (0.00164 mg). During the process of gradually

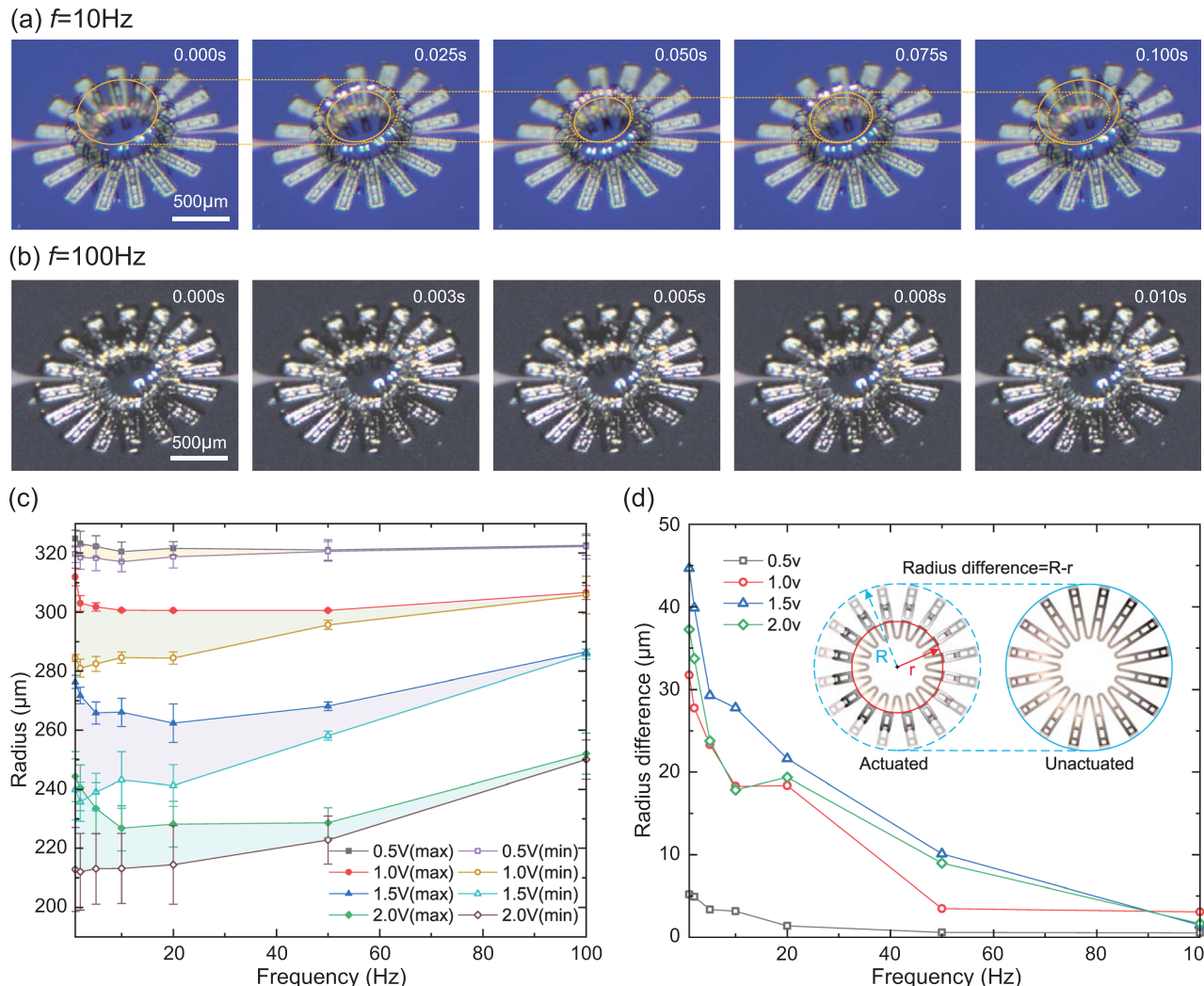


FIG. 4. Composite of video frames of the micro-gripper responding in one cycle under the applied voltage of 2 V at (a) 10 and (b) 100 Hz. (c) The maximum and the minimum radius of the micro-gripper during the oscillation process under pulse voltages from 1 to 100 Hz. (d) Radius differences under pulse voltages from 1 to 100 Hz.

decreasing the voltage after full contraction, the micro-gripper moved and lifted the particle by 34 μm .

In summary, this paper proposed a bimorph thermal micro-gripper, which was capable of performing precise and rapid response with low driving voltages and power consumed. Fabricated through the MEMS technique, the micro-gripper was able to transform from a planar state to a three-dimensional cage-like structure after release. Experimental results revealed that the micro-gripper was able to be electrically actuated and responded precisely under applied voltages from 0.5 to 1.5 V, and the power consumed was less than 80 mW. The operating temperature of the micro-gripper under the applied voltage below 1.2 V was around the human body temperature, which validated its application prospect in biomedicine. Benefit from the optimized current path due to the embedded circuit design scheme and the high surface-to-volume ratio of ultrathin films obtained by the MEMS technique, the response frequency of the micro-gripper could reach

100 Hz without any active cooling measures. Practical abilities of moving and lifting an object were experimentally demonstrated, indicating a broad application prospect of the proposed micro-gripper in biomedicine, micromanipulation, micro-robots, and other fields. According to Lee,³⁹ a corrugated-trench beam design method is validated to be effective in changing the local stiffness of the curved beam, which can be further applied in future work to optimize the internal configuration of the micro-gripper to extend its applicability to targets with different shapes. Future work will also focus on avoiding the impact of the anelasticity of the material on the response performance of the micro-gripper, improving the driving force and the driving distance of the micro-gripper by using the shape memory effect of the nitinol, as well as exploring the insulating layers and wireless energy supplement for the micro-gripper to realize its ability to work remotely in the aqueous environment, such as human body.

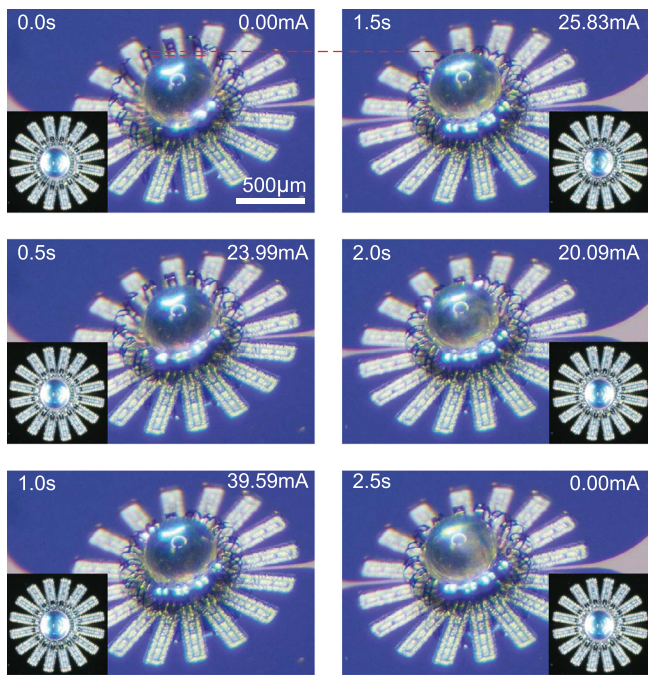


FIG. 5. Composite of video frames showing a micro-gripper grabbing and lifting a SiO_2 particle.

AUTHOR DECLARATIONS

Conflict of Interest

The authors have no conflicts to disclose.

Author Contributions

Xusheng Hui: Conceptualization (lead); Data curation (lead); Formal analysis (lead); Investigation (lead); Methodology (lead); Validation (lead); Visualization (lead); Writing – original draft (lead); Writing – review and editing (equal). **Jianjun Luo:** Conceptualization (equal); Funding acquisition (equal); Investigation (equal); Methodology (equal); Resources (equal); Supervision (equal); Writing – review and editing (equal). **Xinliang Wang:** Investigation (supporting); Methodology (supporting); Validation (supporting); Writing – review and editing (supporting). **Rong Wang:** Data curation (equal); Formal analysis (equal); Writing – original draft (supporting); Writing – review and editing (supporting). **Hao Sun:** Conceptualization (equal); Data curation (equal); Methodology (equal); Resources (equal); Supervision (equal); Writing – original draft (equal); Writing – review and editing (equal).

DATA AVAILABILITY

The data that support the findings of this study are available from the corresponding authors upon reasonable request.

REFERENCES

- ¹W. G. Bircher, A. S. Morgan, and A. M. Dollar, *Sci. Rob.* **6**, eabd2666 (2021).
- ²U. Kim, D. Jung, H. Jeong, J. Park, H.-M. Jung, J. Cheong, H. R. Chol, H. Do, and C. Park, *Nat. Commun.* **12**, 7177 (2021).
- ³W. Ruotolo, D. Brouwer, and M. R. Cutkosky, *Sci. Rob.* **6**, eabi9773 (2021).
- ⁴J. Peak, I. Cho, C. Ru, and J. Kim, *Sci. Reports* **5**, 10768 (2015).
- ⁵T. Jin, Z. Sun, L. Li, Q. Zhang, M. Zhu, Z. Zhang, G. Yuan, T. Chen, Y. Tian, X. Hou, and C. Lee, *Nat. Commun.* **11**, 5381 (2020).
- ⁶M. Zhang, G. Li, X. Yang, W. Xiao, T. Yang, and T.-W. Wong, *Smart Mater.* **27**, 095016 (2018).
- ⁷T. Park, K. Kim, S.-R. Oh, and Y. Cha, *Soft Rob.* **7**, 68 (2020).
- ⁸N. Kellaris, P. Rothemund, Y. Zeng, S. K. Mitchell, G. M. Smith, K. Jayaram, and C. Keplinger, *Adv. Sci.* **8**, 2100916 (2021).
- ⁹S. Zhang, J. Wang, K. Hayashi, and F. Sassa, *Sci. Rep.* **11**, 20015 (2021).
- ¹⁰J. Zhu, X. Liu, Q. Shi, T. He, Z. Sun, X. Guo, W. Liu, O. B. Sulaman, B. Dong, and C. Lee, *Micromachines* **11**, 7 (2019).
- ¹¹S. Shian, K. Bertoldi, and D. R. Clarke, *Adv. Mater.* **27**, 6814 (2015).
- ¹²O. M. Wani, H. Zeng, and A. Priimagi, *Nat. Commun.* **8**, 15546 (2017).
- ¹³A. Lendlein and O. E. C. Gould, *Nat. Rev. Mater.* **4**, 116 (2019).
- ¹⁴Y. Roh, M. Kim, S. M. Won, D. Lim, I. Hong, S. Lee, T. Kim, C. Kim, D. Lee, S. Im, G. Lee, D. Kim, D. Shin, D. Gong, B. Kim, S. Kim, S. Kim, H. K. Kim, B.-K. Koo, S. Seo, J.-S. Koh, D. Kang, and S. Hah, *Sci. Rob.* **6**, eabi6774 (2021).
- ¹⁵Y. Lu and C.-J. Kim, in *Boston TRANSDUCERS'03, Digest of Technical Papers* (IEEE, 2003), p. 276.
- ¹⁶H. Li, G. Go, S. Y. Ko, J.-O. Park, and S. Park, *Smart Mater. Struct.* **25**, 027001 (2016).
- ¹⁷E. Gultepe, J. S. Randhawa, S. Kadam, S. Yamanaka, F. M. Selaru, E. J. Shin, A. N. Kalloo, and D. H. Gracias, *Adv. Mater.* **25**, 514 (2013).
- ¹⁸N. Bassik, A. Braffman, A. M. Zarafshar, M. Jamal, D. Luvsanjav, F. M. Selaru, and D. H. Gracias, *J. Am. Chem. Soc.* **132**, 16314 (2010).
- ¹⁹J. C. Breger, C. K. Yoon, R. Xiao, H. R. Kwag, M. O. Wang, J. P. Fisher, T. D. Nguyen, and D. H. Gracias, *ACS Appl. Mater. Interfaces* **7**, 3398 (2015).
- ²⁰H. Jia, E. Mailand, J. Zhou, Z. Huang, G. Dietler, J. Kolinski, X. Wang, and M. Sakar, *Small* **15**, 1803870 (2019).
- ²¹P. Pan, W. Wang, C. Ru, Y. Sun, and X. Liu, *J. Micromech. Microeng.* **27**, 123003 (2017).
- ²²G. Stoychev, N. Puretskiy, and L. Ionov, *Soft Matter* **7**, 3277 (2011).
- ²³A. Ghosh, Y. Liu, D. Artemov, and D. H. Gracias, *Adv. Healthcare Mater.* **10**, 2000869 (2021).
- ²⁴A. S. Gladman, E. A. Matsumoto, R. G. Nuzzo, L. Mahadevan, and J. A. Lewis, *Nat. Mater.* **15**, 413 (2016).
- ²⁵J. Zheng, P. Xiao, X. Le, W. Lu, P. Théato, C. Ma, B. Du, J. Zhang, Y. Huang, and T. Chen, *Mater. Chem. C* **6**, 1320 (2018).
- ²⁶Z. Zhang, Z. Chen, Y. Wang, J. Chi, Y. Wang, and Y. Zhao, *Small Methods* **3**, 1900519 (2019).
- ²⁷M. Ranucci, T. Laddomada, M. Ranucci, and E. Baryshnikova, *Physiol. Rep.* **2**, e12065 (2014).
- ²⁸G.-K. Lau, J. Yang, B. Thubthimthong, N.-B. Chong, C. P. Tan, and Z. He, *Appl. Phys. Lett.* **101**, 033108 (2012).
- ²⁹P. Pitchappa, C. P. Ho, Y.-S. Lin, P. Kropelnicki, C.-Y. Huang, N. Singh, and C. Lee, *Appl. Phys. Lett.* **104**, 151104 (2014).
- ³⁰S. Zhang, K. Liu, M. Xu, and S. Shen, *Appl. Phys. Lett.* **111**, 082904 (2017).
- ³¹G.-K. Lau, K.-R. Heng, A. S. Ahmed, and M. Shrestha, *Appl. Phys. Lett.* **110**, 182906 (2017).
- ³²N. Kohls, I. Abdeally, B. P. Ruddy, and Y. C. Mazumder, *Lett. Dyn. Sys. Control* **1**, 031011 (2021).
- ³³Q. Shi, Z. Yu, H. Wang, T. Sun, Q. Huang, and T. Fukuda, *IEEE Trans. Nanotechnol.* **17**, 657 (2018).
- ³⁴Q. Wang, Y.-T. Li, T.-Y. Zhang, D.-Y. Wang, Y. Tian, J.-C. Yan, H. Tian, Y. Yang, F. Yang, and T.-L. Ren, *Appl. Phys. Lett.* **112**, 133902 (2018).
- ³⁵Y. Q. Fu, J. K. Luo, S. E. Ong, S. Zhang, A. J. Flewitt, and W. I. Milne, *J. Micromech. Microeng.* **18**, 035026 (2008).
- ³⁶J. J. Gill, D. T. Chang, L. A. Momoda, and G. P. Carman, *Sens. Actuators, A* **93**, 148 (2001).
- ³⁷S. Timoshenko, *J. Opt. Soc. Am.* **11**, 233 (1925).
- ³⁸X. Huang, K. Kumar, M. K. Jawed, A. M. Nasab, Z. Ye, W. Shan, and C. Majidi, *Adv. Mater. Technol.* **4**, 1800540 (2019).
- ³⁹C. Lee, Y.-J. Lai, C.-Y. Wu, Y.-S. Lin, M. H. Tasi, R.-S. Huang, and M.-S. Lin, *Jpn. J. Appl. Phys., Part 1* **43**, 3906 (2004).